Draft version May 8, 2026
Typeset using LaTeX **twocolumn** style in AASTeX631

The δ Scuti pulsator occurrence as a function of age, $T_{\rm eff}$, rotation, and metallicity

Ian Berry,[1] Daniel Huber,[1] Yaguang Li,[1] Daniel Hey,[1] Timothy R. Bedding,[2] and Simon J. Murphy[3]

[1] *Institute for Astronomy, University of Hawai'i, 2680 Woodlawn Drive, Honolulu, HI 96822, USA*
[2] *Sydney Institute for Astronomy, School of Physics, University of Sydney, NSW 2006, Australia*
[3] *Centre for Astrophysics, University of Southern Queensland, Toowoomba, QLD 4350, Australia*

ABSTRACT

Many A- and F- type stars do not display δ Scuti pulsations, despite being located within the instability strip. We use photometry from the TESS Mission to discover and study δ Scuti pulsators in open clusters within 500 pc and with ages between 20 and 900 Myr, which provide a unique opportunity to study δ Scuti pulsators in coeval populations with uniform chemical composition. We measure pulsator occurrence, which corrects the pulsator fraction for incompleteness, across all clusters. We find that clusters younger than 200 Myr tend to exhibit higher occurrence rates, with an average occurrence of 88±3%. The occurrence rates in clusters older than 200 Myr tend to resemble the pulsator fraction of field-star samples, with an average occurrence of 62±3%. In addition, we find that pulsators tend to rotate more rapidly in older clusters than their younger counterparts and that hotter pulsators may stop pulsating earlier than their cooler counterparts. These results show that pulsator occurrence decreases with age and that rapid rotation is critical in maintaining δ Scuti pulsations over time.

1. INTRODUCTION

The δ Scuti pulsators are spectral type A and F stars on or near the main sequence within the classical Cepheid instability strip, spanning effective temperatures ($T_{\rm eff}$) between $\sim 7000-9500$ K. These stars display high-frequency pressure (p) modes due to internal helium ionization zones, which drive radial and non-radial pulsations through periodic changes in opacity known as the κ mechanism (Dupret et al. 2004). Some instability strip stars are hybrid pulsators, displaying both δ Scuti pulsations and low-frequency gravity (g) modes associated with the γ Doradus pulsators (Grigahcène et al. 2010; Hareter et al. 2010; Kurtz et al. 2014; Balona 2018).

The physics of the driving mechanism of pulsations in δ Scuti stars remains poorly understood, with one issue being that some stars within the instability strip seem not to pulsate at all, contrary to theoretical expectations (Dupret et al. 2004, 2005). In addition, stars that appear to fall outside the bounds of the instability strip can show δ Scuti pulsations (e.g. Uytterhoeven et al. 2011; Balona 2018; Murphy et al. 2019; Gaia Collaboration et al. 2023).

Corresponding author: Ian Berry
ianberry@hawaii.edu

As a consequence, much work has been done to measure the pulsator fraction, which is the ratio of pulsators to the total sample size, which appears to vary between different stellar populations. Among field stars, the pulsator fraction varies between 50 and 70% (Murphy et al. 2019; Read et al. 2024; Mani et al. 2025). In general, higher fractions have been measured among brighter stars than among dimmer stars (Read et al. 2024; Mani et al. 2025), suggesting that detection biases/capabilities could affect whether certain instability strip stars appear to pulsate.

The concept of "pulsator occurrence" was introduced by Berry et al. (2025), who used injection and recovery tests and a known δ Scuti amplitude distribution from Murphy et al. (2019) to correct the pulsator fraction for detection biases. This was done using instability strip stars in the 300 Myr old open cluster NGC 3532, where a 63% pulsator occurrence was measured, up from the pulsator fraction of 50%.

Physical factors must also govern whether a star within the instability strip pulsates. δ Scuti pulsations require the presence of a helium ionization zone at a specific depth and temperature ($30,000 - 40,000$ K; Carroll & Ostlie 1996) in the stellar interior to drive pulsations through the κ mechanism. In slowly rotating

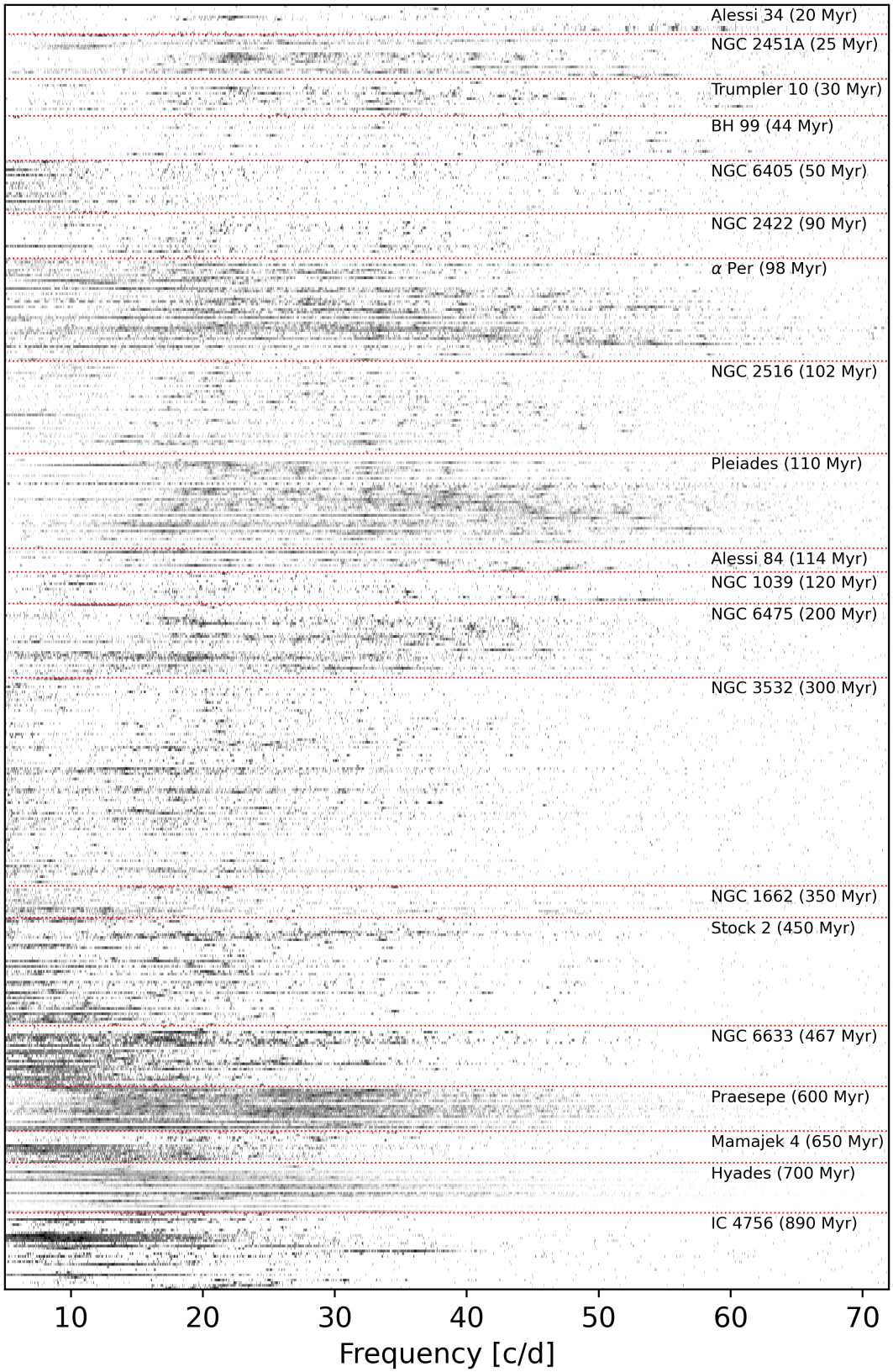

Figure 1. Stacked amplitude spectrum of all δ Scuti pulsators in this study. Clusters are ordered by age (youngest on top). The red dotted lines separate each cluster. Within each cluster, stars are sorted by $T_{\rm eff}$, with the coolest on top. Note the appearance of δ Scuti stars with regular pulsation patterns in the younger ($\lesssim$ 200 Myr) open clusters.

stars, helium can sink out of the ionization zone over time (Baglin et al. 1973), stopping pulsations from the κ mechanism. For a 1.6$\sim$ M$_\odot$ star with a stellar wind, 50% of helium will be depleted from the ionization zone by 100 Myr, and up to 80% by 500 Myr (Théado et al. 2005; Deal et al. 2016). Therefore, the youngest instability strip stars may still have the necessary helium in the ionization zone to drive pulsations, regardless of other stellar parameters.

Rotation can also affect the driving of pulsations. Gravitational settling of helium out of the ionization zone can be counteracted by rotational mixing through rapid rotation (Huang 2004). Recently, Gootkin et al. (2024) found a clear increase in pulsator fraction with increasing rotation rate using a large sample of δ Scuti pulsators. Similar results were found with δ Scuti stars in the Cep-Her Complex (Murphy et al. 2024), the Pleiades (Bedding et al. 2023) and NGC 3532 (Berry et al. 2025).

Chemical composition can affect the driving of pulsations. For example, the metallic-lined Am stars display strong metal absorption lines, and are generally known to be slow rotators, which is thought to allow helium to gravitationally diffuse out of the ionization zone, while allowing metals to rise to the surface through radiation pressure (Pamjatnykh 1974; Dziembowski 1980; Ouazzani et al. 2015). These stars appear to have lower pulsation fractions than their non-metallic-lined counterparts, about 13% (Breger 1970; Guzik et al. 2021; Dürfeldt-Pedros et al. 2024).

The Transiting Exoplanet Survey Satellite (TESS; Ricker et al. 2015) enables a systematic study of δ Scuti stars in open clusters across nearly the entire sky. With extended-mission full-frame-image (FFI) cadences of 10 minutes and 200 seconds, TESS can detect any δ Scuti pulsator regardless of pulsation frequency. These FFIs now cover over 90% of the sky, allowing studies of nearly all nearby ($\lesssim$ 500 pc) δ Scuti stars in both the field and open clusters.

Open clusters and moving groups are an ideal environment for measuring pulsator fractions at a fixed age and chemical composition. Pulsator fractions and occurrences have been measured with TESS in three young stellar populations and one intermediate age open cluster: the Pleiades (100 Myr; Bedding et al. 2023), NGC 2516 (100 Myr; Li et al. 2024), the Cep-Her complex ($\leq$ 80 Myr; Murphy et al. 2024), and NGC 3532 (300 Myr; Berry et al. 2025), where maximum pulsator fractions and occurrences were measured to be $\sim$80%, $\sim$80%, 100%, and 63% respectively. The higher pulsation fractions in the younger populations compared to the pulsator occurrence in the intermediate age cluster NGC 3532 suggest that the pulsation occurrence depends on age.

In this paper, we use TESS photometry to identify and characterize 487 δ Scuti stars in 20 open clusters with ages ranging from tens of Myr to $\sim$ 1 Gyr. We used this sample to investigate the relationship between pulsator occurrence, age, rotation, $T_{\rm eff}$, and metallicity.

2. SAMPLE SELECTION

2.1. *Cluster Selection*

We selected open clusters within 500 pc. The ability to detect δ Scuti stars with TESS decreases significantly at T mag $\gtrsim$ 11, where noise levels become comparable to common δ Scuti pulsation amplitudes ($\gtrsim$ 100 ppm; Read et al. 2024). For the least luminous δ Scuti stars ($L \approx 10\,L_\odot$), T mag = 11 corresponds to a distance of $\sim$500 pc.

We also considered the number of stars in each open cluster, which controls the precision to which we can measure pulsator occurrence through the counting error. Our goal was to keep the counting error around 10% in each cluster. Assuming a pulsator occurrence of 50%, which maximizes the counting error, we would need at least 25 stars total for the counting error to be 10%. Therefore, we only consider clusters with at least 25 members within the de-reddened color range in which we search for δ Scuti stars: $(G_{\rm BP}-G_{\rm RP})_0 = [-0.05, 0.6]$. Finally, we only searched open clusters with ages less than 1 Gyr to avoid clusters where many instability strip stars have evolved off of the main sequence. In total, we found 20 open clusters that are suitable for calculating δ Scuti pulsator occurrence with our desired precision. Properties of all open clusters can be seen in Table 1. Properties of all stars studied in this work are available in Table 2.

2.2. *Cluster Membership*

For most open clusters, we adopt membership catalogs from Hunt & Reffert (2023, 2024), who performed a blind census of Galactic open clusters using Gaia DR3 (Vallenari et al. 2023) astrometry and the Hierarchical Density-Based Spatial Clustering of Applications with Noise algorithm (HDBSCAN; McInnes et al. 2017). Hunt & Reffert (2023, 2024) provide membership probabilities along with a flag identifying candidates that lie within the estimated tidal radius of each cluster, computed following King (1962).

For each cluster, we searched for δ Scuti pulsators among candidate members with this tidal-radius flag set to true. By construction, all stars within the tidal radius have membership probabilities greater than 50%. As noted by Hunt & Reffert (2024), candidates with

Table 1. Properties of the open clusters used in this work. Equatorial coordinates and distances are taken from Hunt & Reffert (2023, 2024). Cluster ages and uncertainties are adopted either from the median values reported by Hunt & Reffert (2023, 2024) or from the literature. Metallicities are taken from Zhang et al. (2024) or from the literature. Clusters with no measured metallicity (i.e. Alessi 34 and Alessi 84) are assumed to be solar. $N_{\delta\,\mathrm{Sct}}$ is the number of δ Scuti stars.

Cluster	α [°]	δ [°]	Distance [pc]	Age [Myr]	[Fe/H]	$N_{\delta\,\mathrm{Sct}}$	Occurrence [%]	Ref.
Alessi 34	120.062	-50.655	485	20^{+12}_{-9}	···	11	86±14	1
NGC 2451A	115.971	-38.241	190	25^{+22}_{-12}	-0.11	17	93^{+7}_{-13}	1,2,3
Trumpler 10	131.937	-42.534	428	30^{+30}_{-20}	-0.12	14	77±13	1,4,5
BH 99	159.554	-59.109	440	44^{+38}_{-19}	0.00	17	100^{+0}_{-14}	1,6
NGC 6405	265.067	-32.228	451	50^{+38}_{-21}	0.07	20	100^{+0}_{-15}	1,7
α Per	51.332	49.119	173	98 ± 2	0.03	39	69±8	1,8,9
NGC 2516	119.521	-60.793	407	102 ± 15	-0.08	35	76±12	1,10,11
NGC 2422	114.169	-14.493	468	107^{+88}_{-45}	-0.05	17	95^{+5}_{-16}	1,10
Pleiades	56.680	24.108	134	110	0.03	36	86±7	1,12,13
Alessi 84	110.510	55.384	198	115^{+89}_{-50}	···	9	91^{+9}_{-16}	1,2
NGC 1039	40.548	42.722	489	120^{+108}_{-49}	0.00	12	89^{+11}_{-18}	1,9
NGC 6475	268.476	-34.828	275	200 ± 50	0.03	28	73±9	1,14
NGC 3532	166.394	-58.694	471	300 ± 100	-0.07	79	59±6	1,15,16,17
NGC 1662	72.114	10.904	404	350^{+236}_{-125}	-0.03	12	65±14	1,9
Stock 2	33.850	59.577	370	450 ± 150	-0.07	41	41±8	1,18
NGC 6633	276.805	6.559	389	550^{+50}_{-100}	-0.15	23	61±10	1,9,19
Praesepe	130.088	19.666	183	589^{+13}_{-26}	0.19	17	73±11	1,9,20
Mamajek 4	276.371	-50.637	444	650	0.09	12	49±15	1,9,21
Hyades	66.709	16.081	47	676^{+13}_{-30}	0.15	19	70±11	1,9,20
IC 4756	279.627	5.437	466	890 ± 70	0.09	29	67±10	1,9,22

References: (1) Hunt & Reffert (2023, 2024); (2) Liu et al. (2025); (3) Hünsch et al. (2003) (4) Netopil et al. (2016) (5) Pamos Ortega et al. (2023); (6) Piecka & Paunzen (2021); (7) Kılıçoğlu et al. (2016); (8) Pamos Ortega et al. (2022); (9) Zhang et al. (2024); (10) Bailey et al. (2018); (11) Li et al. (2024); (12) Bedding et al. (2023); (13) Soderblom et al. (2009); (14) Villanova et al. (2009); (15) Clem et al. (2011); (16) Fritzewski et al. (2019); (17) Berry et al. (2025); (18) Alonso-Santiago et al. (2021); (19) Brogaard et al. (2025); (20) Gossage et al. (2018); (21) Roselli et al. (2023); (22) Strassmeier et al. (2015);

membership probabilities below 50% are consistently associated with low-quality memberships.

For three open clusters, we adopted membership catalogs from Liu et al. (2025), who revised the Hunt & Reffert (2023) catalogs to account for projection effects that can be significant for clusters within 200 pc. The clusters are NGC 2451A, α Per (Melotte 20), and Alessi 84, all of which exhibit substantially larger membership populations in the updated analysis compared to the original Hunt & Reffert (2023) catalogs.

Three of the open clusters analyzed here have been previously studied, with their δ Scuti pulsators already identified. We therefore did not perform an independent search for the δ Scuti stars in these clusters and instead adopted the published classifications. The clusters are the Pleiades (Bedding et al. 2023), NGC 2516 (Li et al. 2024), and NGC 3532 (Berry et al. 2025). Table 1 provides basic properties of all open clusters studied here.

2.3. *TESS Photometry*

We used photometry from TESS to identify δ Scuti pulsators in open clusters. We used the Full-Frame-Images (FFIs) from the extended missions, with cadences of 10-minutes and 200-seconds in the first and second extended missions, respectively. We also used 20-second and 2-minute cadence targeted observations when available.

For all but two open clusters, we used TESS light curves available from the Mikulski Archive for Space Telescopes (MAST)[1]. Because FFI photometry may be reduced by multiple pipelines for a given sector and cadence, we adopt a priority scheme. We first selected FFI light curves processed by the TESS Science Processing Operations Center pipeline (TESS-SPOC; Caldwell et al. 2020). If TESS-SPOC products are not available, we instead used light curves from the Quick-Look Pipeline (QLP; Huang et al. 2020).

[1] https://archive.stsci.edu/

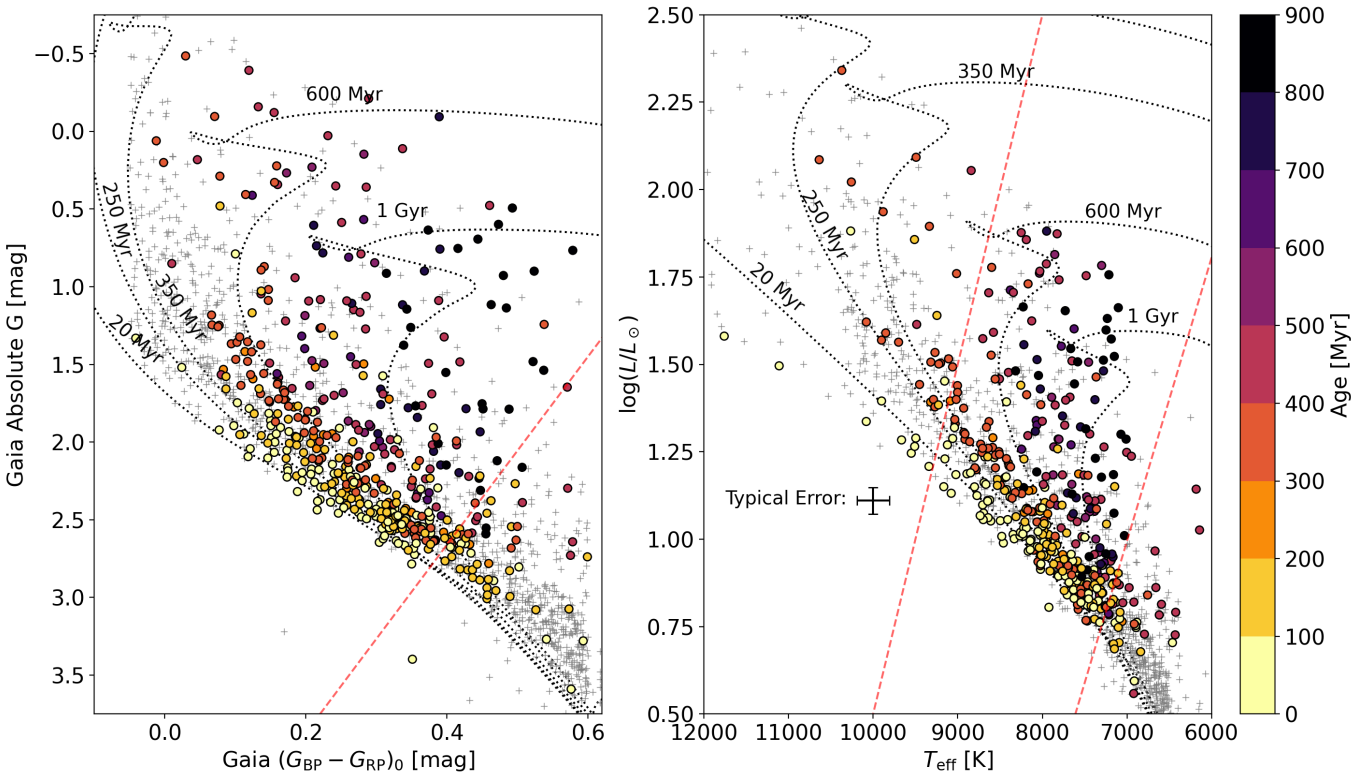

Figure 2. Gaia CMD (left panel) and HR diagram (right panel) for all clusters studied in this work. Color-mapped points are δ Scuti pulsators, and colors show age. Gray crosses are non-detections. The black dotted curves show 40% critical rotation MIST isochrones (Dotter 2016; Choi et al. 2016) at various ages. In the left panel, the red dashed line shows the empirical red instability strip edge from Gootkin et al. (2024). In the right panel, the red dashed lines show the empirical bounds of the instability strip from Murphy et al. (2019).

The light curves were downloaded and processed using the LightKurve Python package (Lightkurve Collaboration et al. 2018). We performed outlier rejection, normalization, NaN removal, and flattening of all light curves using the methods provided in LightKurve (Lightkurve Collaboration et al. 2018).

We used TESS-Gaia Light Curves (TGLCs; Han & Brandt 2023) for the open clusters Stock 2 and NGC 3532. Specifically, we used the same light curves for NGC 3532 as those used by Berry et al. (2025) to mitigate the effects of blending in the crowded field around NGC 3532. We generated our own TGLCs for Stock 2 members, as reduced light curves for a large fraction of Stock 2 members were not readily available on MAST. To do this, we used the `quick_lc.tglc_lc` method from the TGLC Python package. For every star searched, light curves from each unique sector and cadence pair were stitched together into one combined light curve.

We calculated amplitude spectra for all individual sectors of photometry, as well as for all sector-combined light curves using the `LombScargle` method from the AstroPy Python package (Astropy Collaboration et al. 2013, 2018, 2022). Ultimately, we used the sector-combined amplitude spectra to search for δ Scuti pulsators. The amplitude spectra for all δ Scuti stars found in this work are shown in Figure 1.

2.4. *Photometric Quality Cuts*

For each cluster, we automatically discarded poor-quality photometry on a star-by-star, sector-by-sector basis prior to constructing sector-combined light curves. We estimated the noise level in each amplitude spectrum by measuring the mean amplitude within a quiet, high-frequency region within 95% of the Nyquist frequency. This was then compared to the expected noise level derived from simulated light curves and amplitude spectra, generated using photon noise estimates from the TICGEN Python package (Jaffe & Barclay 2017; Stassun et al. 2018).

For each star and sector, we computed the ratio of the measured noise to the expected noise. Photometry with noise ratios exceeding the 95th percentile of all stars and sectors was discarded. This procedure is performed independently for each cadence.

2.5. *Interstellar Reddening*

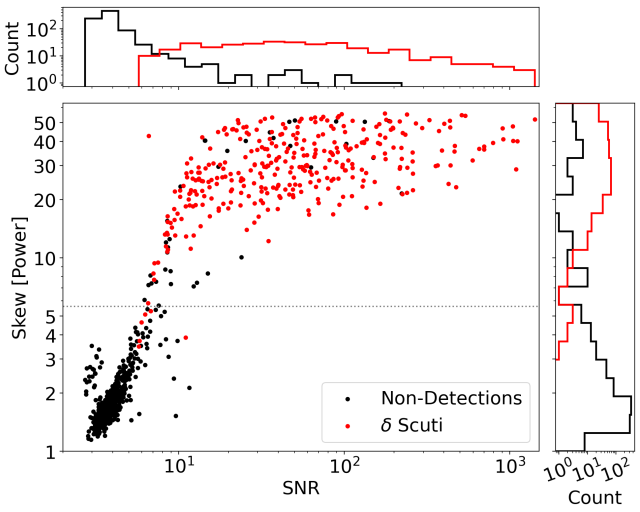

Figure 3. Scatter plot of log skewness vs. maximum SNR. Stars identified as δ Scuti pulsators are in shown as the red points, and non-detections are shown as the black points. The distributions of log skewness and SNR for δ Scuti pulsators and non-detections are shown along each axis, with the same color scheme as the scatter plot. The gray dotted line marks log skewness = 0.75, which is the lower limit used when conducting the injection and recovery tests described in §3.3. This plot does not include stars in the Pleiades, NGC 2516, and NGC 3532, where the δ Scuti stars were identified in previous literature (Bedding et al. 2023; Li et al. 2024; Berry et al. 2025, respectively).

For each cluster, we de-reddened the Gaia $G_{\rm BP} - G_{\rm RP}$ using the median A_V values provided in the cluster member catalogs from (Hunt & Reffert 2023, 2024). We find $E(B-V)$ assuming an extinction law with $R_V = 3.1$. We then estimate $E(G_{\rm BP} - G_{\rm RP}) = E(B-V)/0.76$, found from Table 2 of Wang & Chen (2019). Dereddening is performed before any color constraints are applied to the cluster catalogs. We also corrected for extinction using the same A_V values.

3. CALCULATING PULSATOR OCCURRENCE

3.1. *δ Scuti Identification*

The first step to calculate the pulsator occurrence in an open cluster is to identify δ Scuti pulsators. We followed a similar method from Murphy et al. (2019), by using the skewness of the distribution of peak amplitudes, which will be systematically larger for δ Scuti stars than for stars with no high-frequency variability. This is slightly different from the method used by Murphy et al. (2019), who calculated the skewness using all Fourier amplitudes. In previous literature, a fixed lower frequency boundary (such as 5 $\rm d^{-1}$; Murphy et al. 2019; Gootkin et al. 2024) was set in order to avoid false positives from sources of rotational modulation or γ Doradus (Dor) pulsations (Kaye et al. 1999). For this work, we used a variable lower frequency boundary, set by the empirical δ Scuti period-luminosity relation from Barac et al. (2022) (their equation 4), which is thought to follow the frequency of the fundamental mode.

However, we also confirmed all stars that could be δ Scuti pulsators by visually inspecting the amplitude spectra of stars with log skewness ≥ 0.4. A Gaia CMD and HR diagram showing all δ Scuti stars and non-detections is shown in Figure 2. The distributions of log skewness and maximum signal-to-noise ratio (SNR) for all observed stars are shown in Figure 3.

To validate that we properly identified the δ Scuti pulsators in an open cluster, we plot the maximum amplitude vs. $T_{\rm eff}$. Pulsators typically have a maximum amplitude of order unity mmag. We did not correct the maximum amplitudes for apodization, whereas Mani et al. (2025) applied such a correction. The non-pulsators should form a "non-detection ridge", presumably due to white noise, which increases with cooler, dimmer stars in an open cluster. This plot for the open cluster NGC 6475 (Messier 7) is shown in panel (a) of Figure 4.

3.2. *Measuring Pulsator Fraction Over $T_{\rm eff}$*

The next step involved measuring the pulsator fraction as a continuous function of $T_{\rm eff}$. In previous work, the pulsator fraction across the instability strip was measured discretely by binning in apparent magnitude or color (e.g. Bedding et al. 2023; Gootkin et al. 2024; Read et al. 2024; Murphy et al. 2024; Mani et al. 2025; Berry et al. 2025). However, given that we now aim to compare pulsator occurrences across multiple different stellar populations, it is reasonable to work with fundamental stellar parameters such as $T_{\rm eff}$, rather than photometric parameters, as was done for Kepler by Murphy et al. (2019). We used $T_{\rm eff}$ values from the TESS Input Catalog (TIC; Stassun et al. 2019).

By observing δ Scuti pulsators separated into coeval, equal-metallicity populations, we can study how pulsator occurrence changes as a function of age, metallicity, and $T_{\rm eff}$. Rather than discretely binning over color or $T_{\rm eff}$, we measured pulsator occurrence as a continuous function of $T_{\rm eff}$, avoiding ambiguities associated with binning. We estimated pulsator fraction as a function of $T_{\rm eff}$ using a Gaussian kernel given by:

$$w_i(T_{\rm eff}, \sigma) = \frac{1}{\sqrt{2\pi}\sigma} \exp\left[\frac{-(T_{\rm eff} - T_{{\rm eff},i})^2}{2\sigma^2}\right], \quad (1)$$

where $T_{\rm eff}$ is the effective temperature where the fraction is to be evaluated, and $T_{{\rm eff},i}$ is the effective temperature

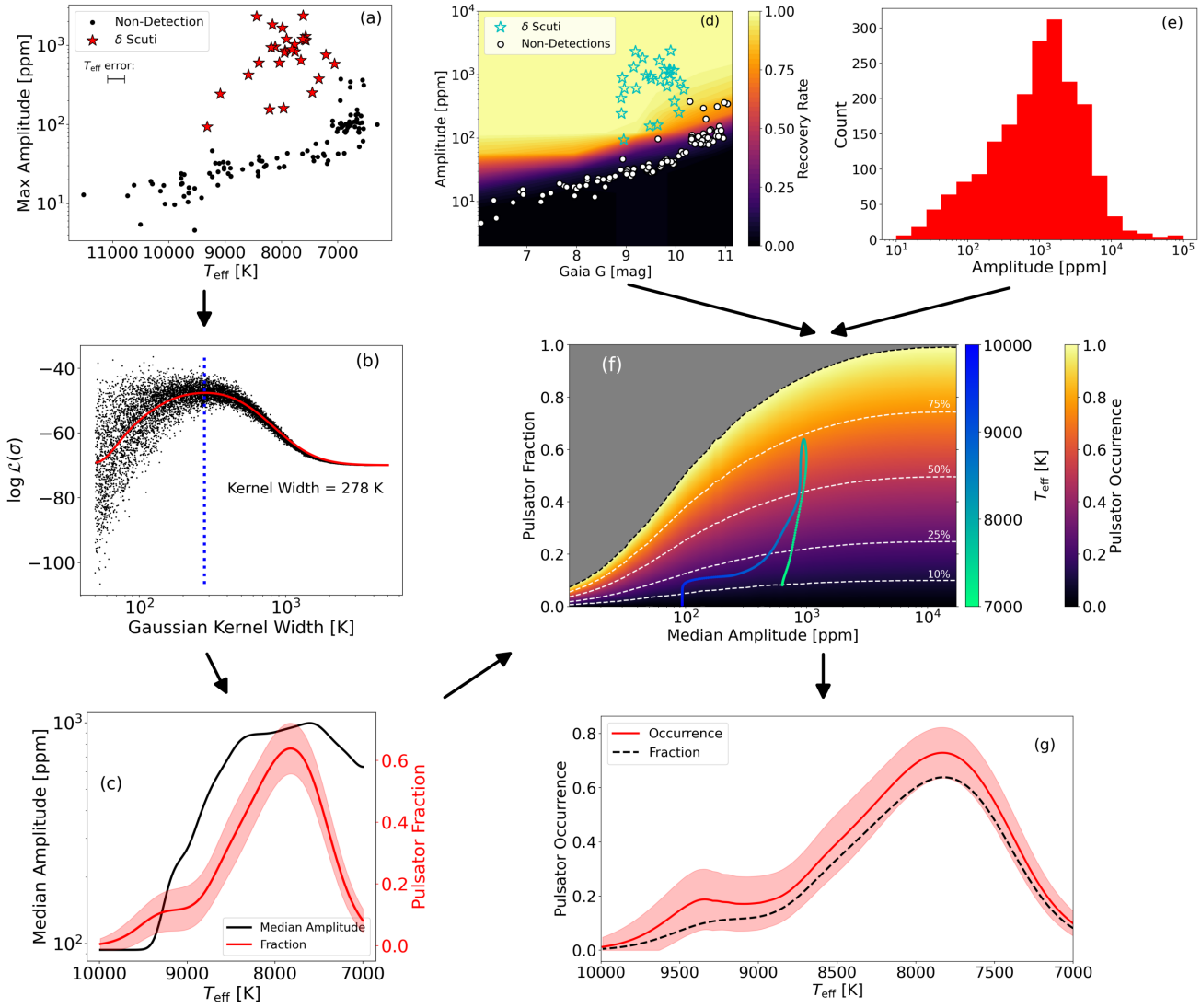

Figure 4. Flowchart illustrating the procedures described in §3 for the open cluster NGC 6475. Panel (a) shows the maximum amplitude vs. $T_{\rm eff}$. Red stars indicate δ Scuti pulsators, black points show non-detections. Panel (b) shows the log-likelihood of the Bernoulli distribution (i.e. Equation 3) as a function of the Gaussian kernel width from a Monte Carlo simulation. The red curve is the binned and smoothed log-likelihood, and the blue dotted line indicates the kernel width that maximizes the log-likelihood. Panel (c) shows the median amplitude and pulsator fraction as functions of $T_{\rm eff}$, using the optimized kernel width. Panel (d) shows δ Scuti recovery rates as a function of amplitude and apparent Gaia G magnitude. Cyan stars show δ Scuti stars, white circles show non-detections. The background colors show recovery rate. Panel (e) shows the δ Scuti amplitude distribution for all observed δ Scuti stars from Kepler (Murphy et al. 2019). Panel (f) shows the pulsator occurrence as a function of pulsator fraction and median amplitude. The inferno color-map shows the pulsator occurrence. The median amplitudes and pulsator fractions from panel (c) are over-plotted as the cyan and blue curve, which tracks $T_{\rm eff}$. Panel (g) shows the resulting pulsator occurrence as a function of $T_{\rm eff}$ as the red curve. Pulsator fraction is also shown again as the black dashed curve. The red shaded region shows the counting error.

of one star in the sample. The kernel width is given by σ. The pulsator fraction, f, for a given $T_{\rm eff}$ and σ was found by:

$$f(T_{\rm eff},\sigma) = \frac{\sum_{i=1}^{N} p_i\, w_i(T_{\rm eff},\sigma)}{\sum_{i=1}^{N} w_i(T_{\rm eff},\sigma)}\,, \tag{2}$$

where p_i is a boolean flag ($p_i = 1$ for δ Scuti pulsators, $p_i = 0$ for non-detections), and N is the sample size. The pulsator fraction f is evaluated at every $T_{\rm eff}$ to obtain a continuous function of $T_{\rm eff}$. We computed f over $T_{\rm eff} = 7000$–$10,000$ K.

The fraction is highly dependent on our choice of σ. Smaller σ will lead to a narrower, taller distribution, and vice versa for a larger σ, which will strongly influence our results. Therefore, it was crucial that we chose σ per cluster in a non-biased, unambiguous way, as we expected that the distribution of pulsators and non-pulsators in $T_{\rm eff}$ would change from cluster to cluster.

We optimized for σ by maximizing the likelihood. In this case, we maximized the likelihood of a Bernoulli distribution, given the boolean nature of this problem. Specifically, we maximized:

$$\ln \mathcal{L}(\sigma) = \sum_{i=1}^{N} p_i \ln \hat{f}_i(T_{\rm eff},\sigma) + (1-p_i)\ln[1-\hat{f}_i(T_{\rm eff},\sigma)]\,, \tag{3}$$

where $\hat{f}$ is Equation 2 found via "leave-one-out" (LOO) cross-validation, which we performed such that each star is predicted as either a pulsator or non-pulsator based only on neighboring stars. In other words, $\hat{f}$ is Equation 2 calculated excluding the i-th star, and stops σ from collapsing towards zero. $\hat{f}$ is given by:

$$\hat{f}_i = \frac{\sum_{j\neq i}^{N} p_j\, w_j(T_{\rm eff},\sigma)}{\sum_{j\neq i}^{N} w_j(T_{\rm eff},\sigma)}\,. \tag{4}$$

We calculated Equation 3 in a Monte Carlo simulation with 10,000 trials. In each trial, we varied the $T_{\rm eff}$ of each star within the uncertainties, assuming that they are normally distributed. We randomly drew values for σ from a log-uniform distribution with values from 50-5000 K. After all trials, we binned and smoothed the likelihood, and find the σ corresponding to the maximum likelihood. This σ was then used to calculate Equations 1 and 2. In most open clusters, σ was on the order of hundreds of Kelvin, with an average kernel width of ≈ 360 K across all 20 open clusters. An example of this process in the open cluster NGC 6475 is shown in panel (b) of Figure 4.

The uncertainty on the pulsator fraction, σ_f, at each $T_{\rm eff}$ can be assumed to be the counting error:

$$\sigma_f = \sqrt{\frac{f(1-f)}{N_{\rm eff}}}\,, \tag{5}$$

where f is the pulsator fraction found via Equation 2 and $N_{\rm eff}$ is the effective sample size, found by:

$$N_{\rm eff} = \frac{[\sum_i^N w_i(T_{\rm eff},\sigma)]^2}{\sum_i^N w_i^2(T_{\rm eff},\sigma)}\,, \tag{6}$$

where $w_i(T_{\rm eff},\sigma)$ is found via Equation 1. These errors are propagated when calculating the pulsator occurrence.

Pulsator occurrence also depends on the median δ Scuti pulsation amplitude. We estimate the median amplitude as a continuous function of $T_{\rm eff}$ using a Gaussian kernel with the same width as for the pulsator fraction. Panel (c) of Figure 4 shows both quantities versus $T_{\rm eff}$ for NGC 6475, which we compare to assess how occurrence varies with temperature.

3.3. *Injection and Recovery Tests*

Following Berry et al. (2025), we injected sinusoids into the light curves of the non-detections with amplitudes ranging between 1 and 10^6 ppm, and random frequencies and phase offsets. We calculated the amplitude spectrum of each non-detection with the injected sinusoid, and a recovery was considered when the log skewness was ≥ 0.75. The recovery rate was found by binning over amplitude and apparent magnitude and calculating the fraction of recoveries in each bin. An example of this process for the open cluster NGC 6475 is shown in panel (d) of Figure 4.

3.4. *Calculating Pulsator Occurrence*

In Berry et al. (2025), stars were randomly assigned as pulsators or non-pulsators, with the number of pulsators determined by the chosen pulsator occurrence, set between 0 and 1. Stars classified as pulsators were assigned one random pulsation amplitude drawn from the amplitude distribution found from field δ Scuti stars observed by Kepler (panel (e) of Figure 4; Murphy et al. 2019). The recovery rate for each pulsator was then determined from its apparent magnitude and assigned amplitude, using the injection and recovery tests described in §3.3. The number of recoveries was the sum of the recovery rates, and a pulsator fraction was measured as the number of recoveries over the total sample size. To account for different median amplitudes, this process was repeated for different amplitude distributions, which was handled by shifting the Kepler distribution uniformly in log-space to match the desired median amplitude. The plot resulting from this exercise (i.e. the δ

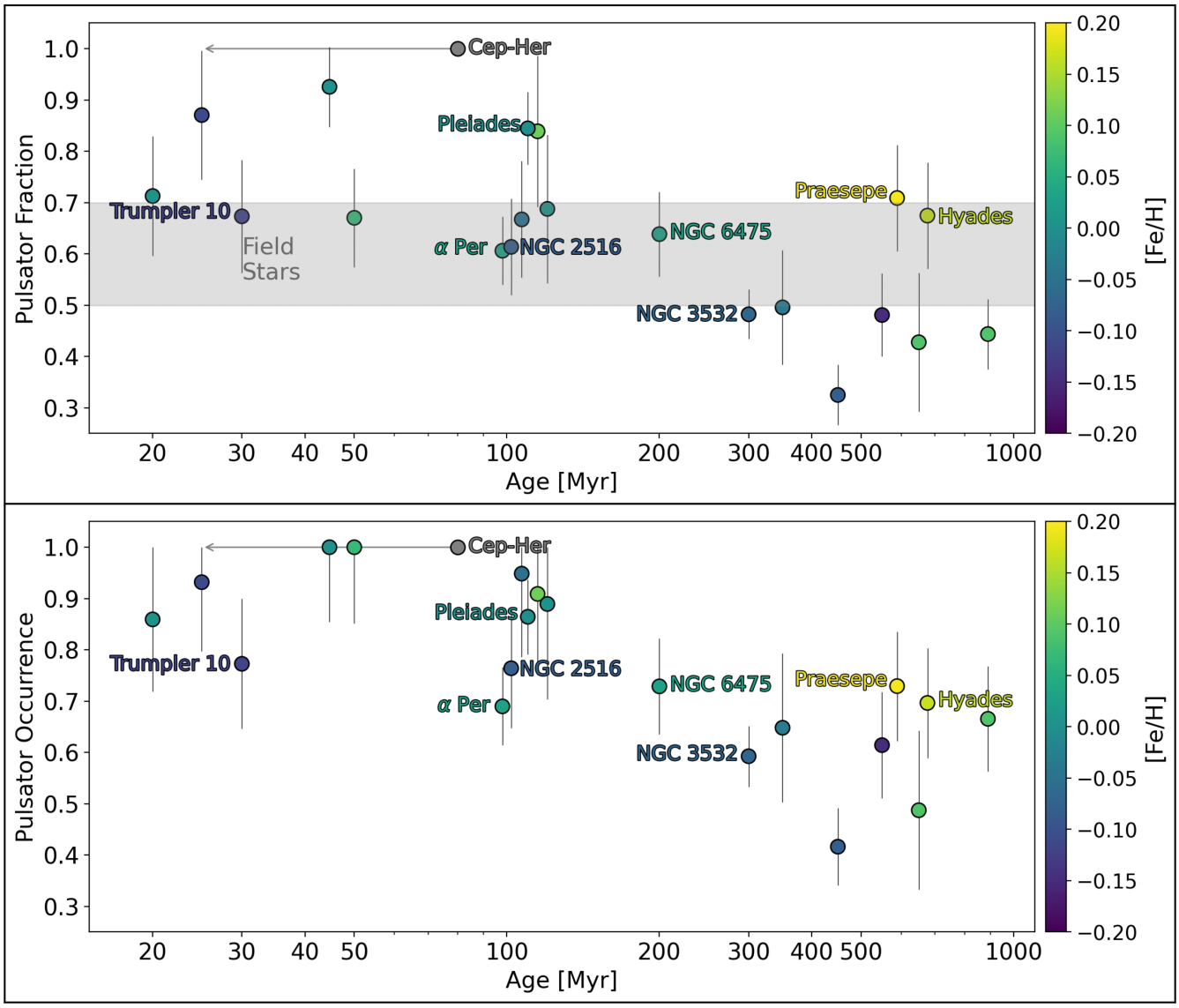

Figure 5. Pulsator fraction (top panel) and pulsator occurrence (bottom panel) as a function of cluster age. Colors show the [Fe/H] of each cluster from previous literature (see Table 1). The gray point with the arrow shows the Cep-Her complex, which is made up of stellar populations with ages between 25 and 80 Myr (Murphy et al. 2024).

Scuti occurrence plot) can be seen in panel (f) of Figure 4, for the open cluster NGC 6475.

The occurrence plot, combined with the functions of median amplitude and pulsator fraction described in §3.2, allows us to find pulsator occurrence as a continuous function over $T_{\rm eff}$ for any open cluster. The resulting pulsator occurrence as a function of $T_{\rm eff}$ for the open cluster NGC 6475 is shown in panel (g) of Figure 4, along with the fraction for comparison. Note that the pulsator occurrence will always be greater than the pulsator fraction.

4. PULSATOR OCCURRENCE, AGE, $T_{\rm EFF}$, AND ROTATION

4.1. *Pulsator Occurrence and Age*

The lower panel of Figure 5 shows the maximum pulsator occurrence in all 20 open clusters as a function of cluster age. For clusters <200 Myr old, we can see that the pulsator occurrence is consistently higher than the pulsator fraction measured in field stars samples (50-70%; Murphy et al. 2019; Read et al. 2024; Mani et al. 2025).

Beyond an age of ∼ 200 Myr, the pulsator occurrence decreases. The average pulsator occurrence in open clusters older than 200 Myr is 62±3% . Meanwhile, the average pulsator occurrence in open clusters younger than 200 Myr is 88±3%. Therefore, the difference in the pul-

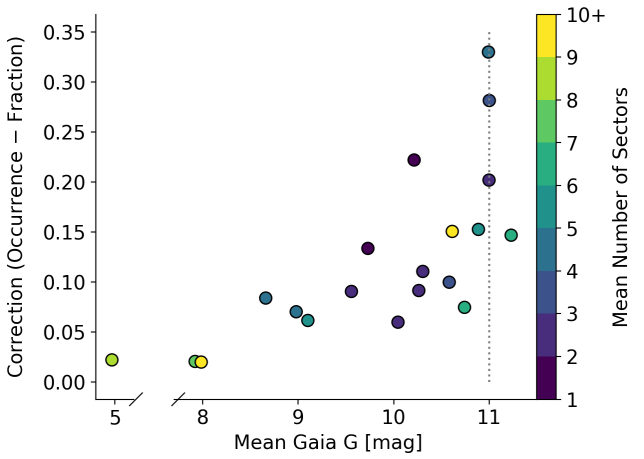

Figure 6. The occurrence correction (defined as the difference between the maximum occurrence and maximum fraction) as a function of the mean Gaia G magnitude in each cluster. Colors show the average number of TESS sectors available for each open cluster.

sator occurrence between young and old open clusters is statistically significant, and shows that the δ Scuti pulsator occurrence decreases with age.

The pulsator occurrence rates in some older clusters are comparable to the pulsator occurrences seen in some clusters less than 100 Myr old. One of these clusters is the ∼600 Myr old Praesepe, which is the most metal-rich cluster studied in this work (Gossage et al. 2018), which suggests that more metal-rich stars may be able to continue pulsating for longer periods of time. The ∼ 700 Myr old Hyades also shows an elevated pulsator occurrence and is also relatively metal-rich (Gossage et al. 2018). However, most clusters studied here have [Fe/H] close to Solar, so additional metal-rich and metal-poor open clusters will need to be studied in the future to solidify any existing trend between pulsator occurrence and metallicity.

When viewing pulsator fraction vs. age, the trend is less clear (Figure 5), as the fraction among young open clusters is not as consistently high as is seen with the pulsator occurrence. The average pulsator fraction for clusters younger than 200 Myr is $74 \pm 4\%$, and while the average for clusters older than 200 Myr is $52 \pm 4\%$. This shows the importance of applying the occurrence correction to the fraction for certain open clusters.

Figure 6 shows the occurrence correction (i.e. the difference between the maximum occurrence and maximum fraction) as function of the mean Gaia G magnitude for each cluster. As expected, we see that larger corrections are warranted when observing fainter samples. We see that the correction can increase rapidly from Gaia $G \geq 10$, which coincides with the detection limit of

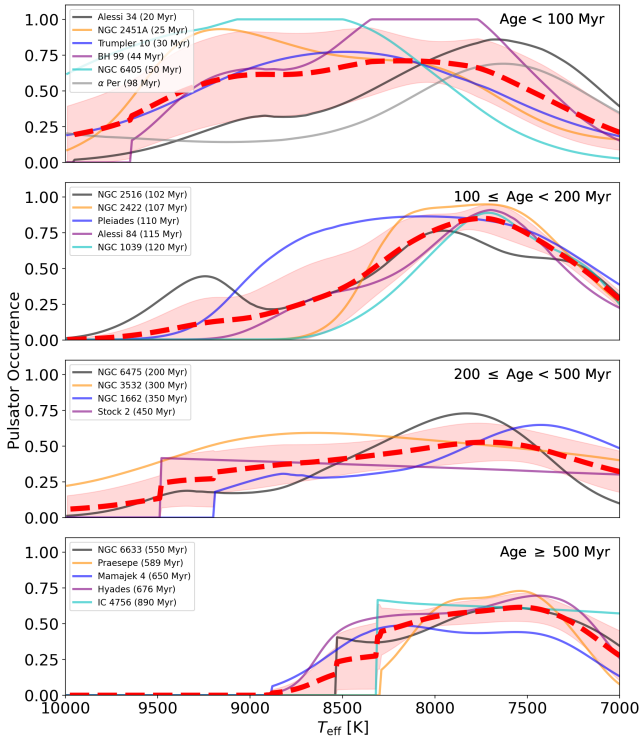

Figure 7. Pulsator occurrence vs. $T_{\rm eff}$ for all open clusters, separated and sorted by age, with the age range listed in each panel. The red dashed curve shows the average pulsator occurrence over $T_{\rm eff}$, and the red shaded region shows the 1σ deviation.

TESS for δ Scuti stars (Read et al. 2024). Furthermore, there is no apparent change in the correction needed between the 8th magnitude clusters (the Pleiades and Praesepe) and the 5th magnitude cluster (the Hyades). This indicates that no completeness correction is necessary for samples brighter than 8th magnitude, and δ Scuti samples in this regime can be treated as effectively complete, in agreement with Read et al. (2024).

4.2. *Pulsator Occurrence and* $T_{\rm eff}$

Although the maximum overall pulsator occurrence in each cluster is a useful global statistic, δ Scuti stars can exist over a ∼ 2000 K range of temperatures, so it is important to also examine how the distribution of δ Scuti pulsators in $T_{\rm eff}$ changes with age. Figure 7 shows the pulsator occurrence vs. $T_{\rm eff}$ for all open clusters studied here, grouped in different age bins, with the mean pulsator occurrence shown as the red dashed curves. In accordance with Figure 5, we can see that the peaks of the functions decrease at older ages. However, we can now see that the pulsator occurrences in hotter δ Scuti stars ($\gtrsim$ 8500 K) appear to be larger in younger open clusters. This suggests that hotter δ Scuti stars may stop pulsating sooner than their cooler counterparts.

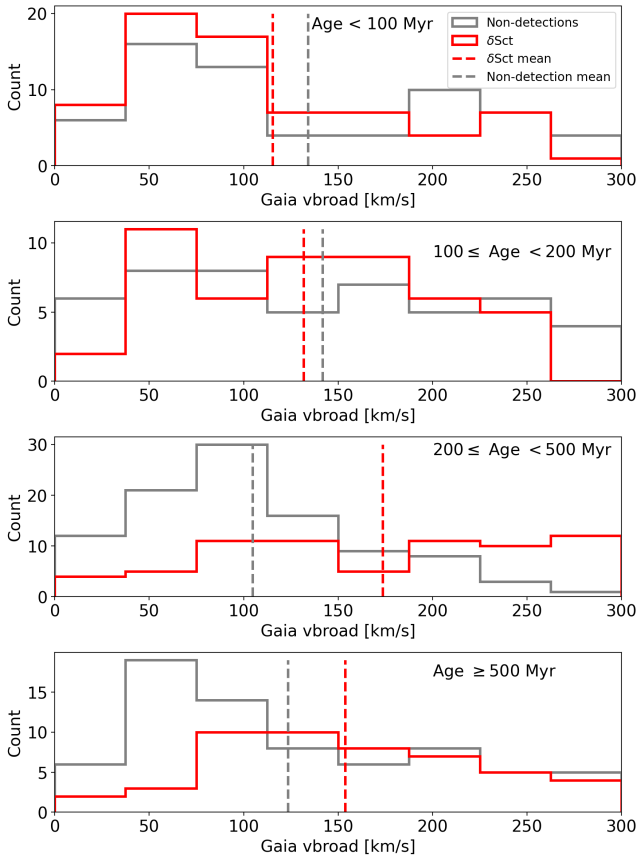

Figure 8. Gaia `vbroad` histograms of the δ Scuti pulsators (red) and non-detections (gray) binned by age, with the youngest stars on top. The red and gray dashed lines show the mean the distributions for the δ Scuti pulsators and non-detections, respectively. These histograms only include stars within the empirical bounds of the instability strip from Murphy et al. (2019).

4.3. *Pulsator Occurrence and Rotation*

Previous work has shown that rotation also affects pulsator occurrence, where faster rotators are more likely to pulsate (Bedding et al. 2023; Gootkin et al. 2024; Murphy et al. 2024; Berry et al. 2025). Therefore, it is important to examine how age and rotation together affect the pulsator occurrence.

We use Gaia `vbroad` as our proxy for rotation, which is an estimation of the projected rotational velocity $v \sin i$ from the Gaia RVS spectrograph (Cropper et al. 2018; Frémat et al. 2023). Murphy et al. (2024) compared the Gaia `vbroad` to cataloged $v \sin i$ values from Zorec & Royer (2012) and found that `vbroad` performs well for velocities between 75 and 200 km s^{-1}, but underestimates the $v \sin i$ of slow rotators ($v \sin i \lesssim 50$ km s^{-1}), and overestimates the $v \sin i$ of rapid rotators ($v \sin i \gtrsim 200$ km s^{-1}). We note that we use the Gaia `vbroad` for all stars, excluding 49 stars in the Pleiades, where $v \sin i$ was measured using spectra from the Center for Astrophysics survey (Torres 2020; Torres et al. 2021; Bedding et al. 2023).

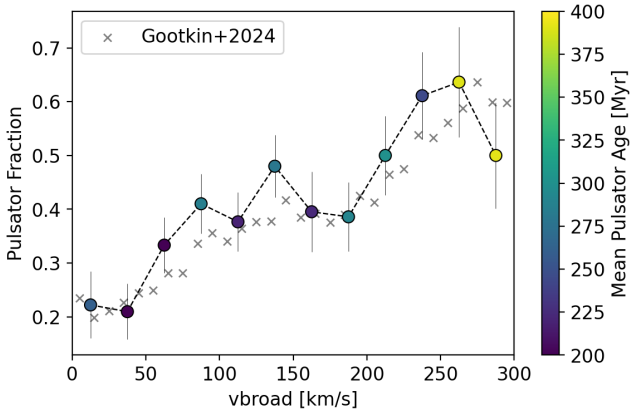

Figure 9. Pulsator fraction vs. Gaia `vbroad`, with colors showing the mean δ Scuti pulsator age in each `vbroad` bin. Results from Gootkin et al. (2024) are shown as the gray crosses.

Figure 8 shows the Gaia `vbroad` distributions for the δ Scuti pulsators and non-detections. On average, δ Scuti pulsators in older clusters rotate more rapidly than those in younger clusters. Together, these trends indicate that older stellar populations have lower overall δ Scuti occurrence, with the remaining pulsators likely persisting due to their rapid rotation.

We plot the pulsator fraction vs. `vbroad` in a similar way to Gootkin et al. (2024) in Figure 9. We binned all stars studied here by `vbroad`, regardless of the cluster to which they belong. As a consequence, we can only measure fraction, since pulsator occurrence can only be inferred in coeval, equidistant populations. In addition, we only considered stars brighter and bluer than the empirical red edge found by Gootkin et al. (2024). Our results agree very well with those found by Gootkin et al. (2024) (gray crosses in Figure 9), in that we see a considerable increase in pulsator fraction with faster rotators. Since we have age information available, we calculated the mean δ Scuti pulsator age within each `vbroad` bin. We find a similar result as in Figure 8; that on average, more slowly rotating pulsators tend to be younger, and older pulsators tend to be more rapidly rotating. This is the opposite of the trend expected in the general stellar population, where stars typically spin-down as they age due to expansion.

We note that Wang et al. (2025) reported an apparent decrease in the rotation velocity of δ Scuti stars with increasing age, based on a sample of field δ Scuti stars observed with LAMOST and TESS. This trend is opposite to what we find here. One possible source of this

discrepancy is the difference in sample selection. We analyze stars in open clusters, whereas Wang et al. (2025) consider field stars, which are known to exhibit different $v \sin i$ and rotation axis inclination distributions (Huang & Gies 2006; Kovacs 2018).

4.4. *Physical Interpretation*

δ Scuti stars pulsate because of a partial helium ionization zone near the surface, which drives pulsations due to periodic changes in opacity (Dupret et al. 2004). If this ionization zone is sufficiently depleted of helium, then δ Scuti pulsations may either have amplitudes too low to be detected, or stop altogether.

It is well known that helium can gravitationally diffuse into deeper layers of stars over time (Baglin et al. 1973). Therefore, it is possible that helium can settle out of the near-surface ionization zone of δ Scuti stars as they age. Models of helium settling in A-type stars (e.g. Théado et al. 2005; Deal et al. 2020) show that helium diffusion occurs quickly relative to the main sequence lifetimes of these stars. Specifically, 50% of helium diffusion can occur by an age of 100 Myr and 80% depletion by 500 Myr. It is still not clear exactly how much depletion would cause a δ Scuti star to stop pulsating. Figure 5 shows a noticeable decrease in the pulsator occurrence in clusters much older than 100 Myr, suggesting that δ Scuti stars may stop pulsating once the helium depletion in the ionization zone exceeds 50%.

Our result in Figure 7 suggests that hotter δ Scuti stars may stop pulsating earlier than cooler stars. In hotter pulsators, the convective helium ionization zone is thinner and located closer to the surface, potentially allowing helium to deplete more rapidly than in cooler stars (Théado et al. 2005). Part of the apparent decline at higher temperatures may also reflect basic stellar evolution, since A-type stars cool as they age and ultimately evolve off the main sequence.

Our results in Figures 8 and 9 demonstrate that age and rotation are closely linked in shaping pulsator occurrence, supporting the idea that helium settling can suppress δ Scuti pulsations. Helium diffusion into deeper stellar layers can be counteracted by rotational mixing, which helps helium remain in the ionization zone over time (Huang 2004). In this scenario, rapid rotators may continue pulsating longer than slow rotators. This is precisely the trend observed in Figure 8. In older clusters, where pulsator occurrence is lower, the remaining δ Scuti stars rotate more rapidly than pulsators in younger clusters, on average. Figure 9 also shows that more slowly rotating pulsators tend to be younger than more rapidly rotating pulsators.

5. CONCLUSIONS & OUTLOOK

We have measured the δ Scuti pulsator occurrence in 20 open clusters to study how the occurrence varies with age, rotation, $T_{\rm eff}$, and metallicity. We obtained the following results:

1. We found that the pulsator occurrence decreases with age, which suggests that δ Scuti stars can stop pulsating over time. The pulsator occurrence in open clusters younger than 200 Myr is consistently high, which an average occurrence of 88±3%. The pulsator occurrence in clusters older than 200 Myr is lower, with an average occurrence of $62 \pm 3\%$.

2. A dependence between the δ Scuti pulsator occurrence and metallicity may exist, with more metal-rich stars maintaining their δ Scuti pulsations over a longer period of time than more metal-poor stars. This trend is tentative, as we did not have many metal-rich clusters in our sample.

3. We found a possible $T_{\rm eff}$-age dependence on the δ Scuti occurrence, where hotter δ Scuti stars ($\gtrsim$ 8500 K) may stop pulsating earlier than their cooler counterparts.

4. We found a link between age, rotation, and the δ Scuti pulsator occurrence, where δ Scuti stars in older open clusters with lower pulsator occurrences are more rapidly rotating than pulsators in younger open clusters with higher pulsator occurrences. This shows that rapid rotation is crucial in maintaining δ Scuti pulsations over the main sequence lifetimes of these stars.

Much more work can be done with δ Scuti stars in open clusters. With TESS, we limited this study to open clusters within 500 pc. Many more populous open clusters exist at further distances (Hunt & Reffert 2023, 2024), which may be excellent candidates for testing and extending the results shown in this work. The δ Scuti pulsator occurrence may be measured in more distant open clusters using the upcoming PLAnetary Transists and Oscillations of Stars high-precision space photometer (PLATO; Rauer et al. 2024), many of which exist within the first field to be observed by PLATO for two years (LOPS2; Nascimbeni et al. 2025). Furthermore, we plan to model the effects of helium diffusion on the δ Scuti pulsator occurrence in the future, using the Yale Rotating Evolution Code (YREC; Larson & Demarque

Table 2. Properties of all stars searched in this work. This table is available in machine-readable format.

Column name	Header	Unit	Description
Open Cluster Common Name	`Common_Name`	-	The common name of the open cluster to which the star belongs
Open Cluster Designation	`Name`	-	Cluster designation used to query the Hunt & Reffert (2023) catalog
Open Cluster Age	`Age`	Myr	-
Gaia DR3 Source ID	`GaiaDR3`	-	-
TESS Input Catalog ID	`TICID`	-	-
Right Ascension (R.A.)	`ra`	$^\circ$	-
Declination (Dec)	`dec`	$^\circ$	-
Parallax	`Plx`	mas	-
Apparent Gaia G magnitude	`Gmag`	mag	-
Apparent TESS magnitude	`Tmag`	mag	-
Absolute Gaia G magnitude	`abs_G`	mag	-
V-band cluster extinction	`Av`	mag	Median A_V from Hunt & Reffert (2023)
Gaia $G_{\rm BP} - G_{\rm RP}$ color	`bp_rp`	mag	-
Dereddened Gaia $G_{\rm BP} - G_{\rm RP}$ color	`bp_rp_0`	mag	-
Gaia RUWE	`ruwe`	-	-
$v \sin i$	`vsini`	$\mathrm{km\,s^{-1}}$	Projected Rotational Velocity from Gaia `vbroad` or Bedding et al. (2023)
$v \sin i$ Error	`vsini_err`	$\mathrm{km\,s^{-1}}$	Error on the projected rotational velocity
Effective Temperature	`Teff`	K	From the TESS Input Catalog (Stassun et al. 2019)
Effective Temperature Error	`s_Teff`	K	”
log Luminosity	`Lum`	$\mathrm{L_\odot}$	”
log Luminosity Error	`s_Lum`	$\mathrm{L_\odot}$	”
TESS Sectors	`num_sectors`	-	Number of TESS sectors used
log Skew	`skew`	-	log skewness of the distribution of peak amplitudes (§3.1)
Maximum Amplitude	`max_amp`	ppt	-
Maximum SNR	`max_snr`	-	SNR of the maximum amplitude
δ Scuti	`dsct`	-	Boolean flag, 1 for δ Scuti stars, 0 for non-detections

1964; Pinsonneault et al. 1989; Demarque et al. 2008; van Saders & Pinsonneault 2013; Pinsonneault et al. 2026).

Beyond pulsator occurrence, δ Scuti stars with regular mode spacings enable precise age estimates for young open clusters ($\lesssim$ 200 Myr) through asteroseismic modeling (e.g. Bedding et al. 2020; Murphy et al. 2023; Gatuam et al. 2026). How other asteroseismic properties, such as pulsation amplitude and frequency, evolve with age and rotation remains to be explored using open clusters.

ACKNOWLEDGMENTS

I.B. and D.H. acknowledge support from the National Aeronautics and Space Administration (80NSSC22K0781). Y.L. acknowledges support from the National Aeronautics and Space Administration (80NSSC25K7904) and the Beatrice Watson Parrent Fellowship. T.R.B and S.J.M. were supported by the Australian Research Council through Laureate Fellowship FL220100117 and Future Fellowship FT2100100485.

This paper includes data collected with the TESS mission, obtained from the MAST data archive at the Space Telescope Science Institute (STScI). Funding for the TESS mission is provided by the NASA Explorer Program. STScI is operated by the Association of Universities for Research in Astronomy, Inc., under NASA contract NAS 5–26555.

DATA AVAILABILITY STATEMENT

The data presented in this paper are available via a machine-readable table. This work used data from the TIC catalog (TESS Team 2018), FFI photometry from TESS Sectors 27 and above (TESS Team 2022), as well as TESS Long (2-minute; TESS Team 2021a) and Fast (20-second; TESS Team 2021b) cadence targeted photometry. The TGLC light curves used for NGC 3532 are available at DOI: 10.5281/zenodo.17402160

REFERENCES

Alonso-Santiago, J., Frasca, A., Catanzaro, G., et al. 2021, A&A, 656, A149, doi: 10.1051/0004-6361/202141747

Astropy Collaboration, Robitaille, T. P., Tollerud, E. J., et al. 2013, A&A, 558, A33, doi: 10.1051/0004-6361/201322068

Astropy Collaboration, Price-Whelan, A. M., Sipőcz, B. M., et al. 2018, AJ, 156, 123, doi: 10.3847/1538-3881/aabc4f

Astropy Collaboration, Price-Whelan, A. M., Lim, P. L., et al. 2022, ApJ, 935, 167, doi: 10.3847/1538-4357/ac7c74

Baglin, A., Breger, M., Chevalier, C., et al. 1973, A&A, 23, 221

Bailey, J. I., Mateo, M., White, R. J., Shectman, S. A., & Crane, J. D. 2018, MNRAS, 475, 1609, doi: 10.1093/mnras/stx3266

Balona, L. A. 2018, Frontiers in Astronomy and Space Sciences, 5, 43, doi: 10.3389/fspas.2018.00043

Barac, N., Bedding, T. R., Murphy, S. J., & Hey, D. R. 2022, MNRAS, 516, 2080, doi: 10.1093/mnras/stac2132

Bedding, T. R., Murphy, S. J., Hey, D. R., et al. 2020, Nature, 581, 147, doi: 10.1038/s41586-020-2226-8

Bedding, T. R., Murphy, S. J., Crawford, C., et al. 2023, ApJL, 946, L10, doi: 10.3847/2041-8213/acc17a

Berry, I., Huber, D., Li, Y., et al. 2025, ApJ, 995, 128, doi: 10.3847/1538-4357/ae18c6

Breger, M. 1970, ApJ, 162, 597, doi: 10.1086/150691

Brogaard, K., Miglio, A., Arentoft, T., et al. 2025, A&A, 702, A265, doi: 10.1051/0004-6361/202449144

Caldwell, D. A., Tenenbaum, P., Twicken, J. D., et al. 2020, Research Notes of the American Astronomical Society, 4, 201, doi: 10.3847/2515-5172/abc9b3

Carroll, B. W., & Ostlie, D. A. 1996, An Introduction to Modern Astrophysics

Choi, J., Dotter, A., Conroy, C., et al. 2016, ApJ, 823, 102, doi: 10.3847/0004-637X/823/2/102

Clem, J. L., Landolt, A. U., Hoard, D. W., & Wachter, S. 2011, AJ, 141, 115, doi: 10.1088/0004-6256/141/4/115

Cropper, M., Katz, D., Sartoretti, P., et al. 2018, A&A, 616, A5, doi: 10.1051/0004-6361/201832763

Deal, M., Goupil, M.-J., Marques, J. P., Reese, D. R., & Lebreton, Y. 2020, A&A, 633, A23, doi: 10.1051/0004-6361/201936666

Deal, M., Richard, O., & Vauclair, S. 2016, A&A, 589, A140, doi: 10.1051/0004-6361/201628180

Demarque, P., Guenther, D. B., Li, L. H., Mazumdar, A., & Straka, C. W. 2008, Ap&SS, 316, 31, doi: 10.1007/s10509-007-9698-y

Dotter, A. 2016, ApJS, 222, 8, doi: 10.3847/0067-0049/222/1/8

Dupret, M. A., Grigahcène, A., Garrido, R., Gabriel, M., & Scuflaire, R. 2004, A&A, 414, L17, doi: 10.1051/0004-6361:20031740

—. 2005, A&A, 435, 927, doi: 10.1051/0004-6361:20041817

Dürfeldt-Pedros, O., Antoci, V., Smalley, B., et al. 2024, A&A, 690, A104, doi: 10.1051/0004-6361/202349076

Dziembowski, W. 1980, in Nonradial and Nonlinear Stellar Pulsation, ed. H. A. Hill & W. A. Dziembowski, Vol. 125, 22–33, doi: 10.1007/3-540-09994-8_2

Frémat, Y., Royer, F., Marchal, O., et al. 2023, A&A, 674, A8, doi: 10.1051/0004-6361/202243809

Fritzewski, D. J., Barnes, S. A., James, D. J., et al. 2019, A&A, 622, A110, doi: 10.1051/0004-6361/201833587

Gaia Collaboration, De Ridder, J., Ripepi, V., et al. 2023, A&A, 674, A36, doi: 10.1051/0004-6361/202243767

Gatuam, A., Murphy, S. J., & Bedding, T. R. 2026, MNRAS, 545, staf2001, doi: 10.1093/mnras/staf2001

Gootkin, K., Hon, M., Huber, D., et al. 2024, ApJ, 972, 137, doi: 10.3847/1538-4357/ad5282

Gossage, S., Conroy, C., Dotter, A., et al. 2018, ApJ, 863, 67, doi: 10.3847/1538-4357/aad0a0

Grigahcène, A., Uytterhoeven, K., Antoci, V., et al. 2010, Astronomische Nachrichten, 331, 989, doi: 10.1002/asna.201011443

Guzik, J. A., Jackiewicz, J., Catanzaro, G., & Soukup, M. S. 2021, arXiv e-prints, arXiv:2107.09479, doi: 10.48550/arXiv.2107.09479

Han, T., & Brandt, T. D. 2023, AJ, 165, 71, doi: 10.3847/1538-3881/acaaa7

Hareter, M., Reegen, P., Miglio, A., et al. 2010, arXiv e-prints, arXiv:1007.3176, doi: 10.48550/arXiv.1007.3176

Huang, C. X., Vanderburg, A., Pál, A., et al. 2020, Research Notes of the American Astronomical Society, 4, 204, doi: 10.3847/2515-5172/abca2e

Huang, R. Q. 2004, A&A, 425, 591, doi: 10.1051/0004-6361:20034245

Huang, W., & Gies, D. R. 2006, ApJ, 648, 580, doi: 10.1086/505782

Hünsch, M., Weidner, C., & Schmitt, J. H. M. M. 2003, A&A, 402, 571, doi: 10.1051/0004-6361:20030268

Hunt, E. L., & Reffert, S. 2023, A&A, 673, A114, doi: 10.1051/0004-6361/202346285

—. 2024, A&A, 686, A42, doi: 10.1051/0004-6361/202348662

Jaffe, T. J., & Barclay, T. 2017, ticgen: A tool for calculating a TESS magnitude, and an expected noise level for stars to be observed by TESS, v1.0.0, Zenodo, doi: 10.5281/zenodo.888217

Kaye, A., Handler, G., Krisciunas, K., Poretti, E., & Zerbi, F. 1999, Publications of the Astronomical Society of the Pacific, 111, 840–844, doi: 10.1086/316399

Kılıçoğlu, T., Monier, R., Richer, J., Fossati, L., & Albayrak, B. 2016, AJ, 151, 49, doi: 10.3847/0004-6256/151/3/49

King, I. 1962, AJ, 67, 471, doi: 10.1086/108756

Kovacs, G. 2018, A&A, 612, L2, doi: 10.1051/0004-6361/201731355

Kurtz, D. W., Saio, H., Takata, M., et al. 2014, MNRAS, 444, 102, doi: 10.1093/mnras/stu1329

Larson, R. B., & Demarque, P. R. 1964, ApJ, 140, 524, doi: 10.1086/147946

Li, G., Aerts, C., Bedding, T. R., et al. 2024, A&A, 686, A142, doi: 10.1051/0004-6361/202348901

Lightkurve Collaboration, Cardoso, J. V. d. M., Hedges, C., et al. 2018, Lightkurve: Kepler and TESS time series analysis in Python, Astrophysics Source Code Library. http://ascl.net/1812.013

Liu, P., Fang, M., Tsai, Y.-L. S., et al. 2025, Revisiting open clusters within 200 pc in the solar neighbourhood with Gaia DR3. https://arxiv.org/abs/2504.08179

Mani, P., Bedding, T. R., Bernizzoni, M., Murphy, S. J., & Hey, D. 2025, MNRAS, 542, 2866, doi: 10.1093/mnras/staf1400

McInnes, L., Healy, J., & Astels, S. 2017, The Journal of Open Source Software, 2, 205

Murphy, S. J., Bedding, T. R., Gautam, A., & Joyce, M. 2023, MNRAS, 526, 3779, doi: 10.1093/mnras/stad2849

Murphy, S. J., Bedding, T. R., Gautam, A., Kerr, R. P., & Mani, P. 2024, MNRAS, 534, 3022, doi: 10.1093/mnras/stae2226

Murphy, S. J., Hey, D., Van Reeth, T., & Bedding, T. R. 2019, MNRAS, 485, 2380, doi: 10.1093/mnras/stz590

Nascimbeni, V., Piotto, G., Cabrera, J., et al. 2025, A&A, 694, A313, doi: 10.1051/0004-6361/202452325

Netopil, M., Paunzen, E., Heiter, U., & Soubiran, C. 2016, A&A, 585, A150, doi: 10.1051/0004-6361/201526370

Ouazzani, R. M., Roxburgh, I. W., & Dupret, M. A. 2015, A&A, 579, A116, doi: 10.1051/0004-6361/201525734

Pamjatnykh, A. A. 1974, Nauchnye Informatsii, 32, 104

Pamos Ortega, D., García Hernández, A., Suárez, J. C., et al. 2022, MNRAS, 513, 374, doi: 10.1093/mnras/stac864

Pamos Ortega, D., Mirouh, G. M., García Hernández, A., Suárez Yanes, J. C., & Barceló Forteza, S. 2023, A&A, 675, A167, doi: 10.1051/0004-6361/202346323

Piecka, M., & Paunzen, E. 2021, A&A, 649, A54, doi: 10.1051/0004-6361/202040139

Pinsonneault, M. H., Kawaler, S. D., Sofia, S., & Demarque, P. 1989, ApJ, 338, 424, doi: 10.1086/167210

Pinsonneault, M. H., van Saders, J. L., Cao, L., et al. 2026, The YREC Stellar Evolution Code: Public Data Release. https://arxiv.org/abs/2603.25792

Rauer, H., Aerts, C., Cabrera, J., et al. 2024, The PLATO Mission. https://arxiv.org/abs/2406.05447

Read, A. K., Bedding, T. R., Mani, P., et al. 2024, MNRAS, 528, 2464, doi: 10.1093/mnras/stae165

Ricker, G. R., Winn, J. N., Vanderspek, R., et al. 2015, Journal of Astronomical Telescopes, Instruments, and Systems, 1, 014003, doi: 10.1117/1.JATIS.1.1.014003

Roselli, E., Curtis, J., Shaham, B., Agüeros, M., & Schuler, S. 2023, in American Astronomical Society Meeting Abstracts, Vol. 241, American Astronomical Society Meeting Abstracts #241, 402.30

Soderblom, D. R., Laskar, T., Valenti, J., & Stauffer, J. R. 2009, in American Astronomical Society Meeting Abstracts, Vol. 214, American Astronomical Society Meeting Abstracts #214, 314.03

Stassun, K. G., Oelkers, R. J., Pepper, J., et al. 2018, AJ, 156, 102, doi: 10.3847/1538-3881/aad050

Stassun, K. G., Oelkers, R. J., Paegert, M., et al. 2019, AJ, 158, 138, doi: 10.3847/1538-3881/ab3467

Strassmeier, K. G., Weingrill, J., Granzer, T., et al. 2015, A&A, 580, A66, doi: 10.1051/0004-6361/201525756

TESS Team. 2018, TESS Input Catalog and Candidate Target List, STScI/MAST, doi: 10.17909/FWDT-2X66

—. 2021a, TESS light curves - all sectors, STScI/MAST

—. 2021b, TESS “fast” light curves - all sectors, STScI/MAST

—. 2022, TESS calibrated full frame images: All sectors, STScI/MAST

Théado, S., Vauclair, S., & Cunha, M. S. 2005, A&A, 443, 627, doi: 10.1051/0004-6361:20052933

Torres, G. 2020, ApJ, 901, 91, doi: 10.3847/1538-4357/abb136

Torres, G., Latham, D. W., & Quinn, S. N. 2021, ApJ, 921, 117, doi: 10.3847/1538-4357/ac1585

Uytterhoeven, K., Moya, A., Grigahcène, A., et al. 2011, A&A, 534, A125, doi: 10.1051/0004-6361/201117368

Vallenari, A., Brown, A. G. A., Prusti, T., et al. 2023, A&A, 674, A1, doi: 10.1051/0004-6361/202243940

van Saders, J. L., & Pinsonneault, M. H. 2013, ApJ, 776, 67, doi: 10.1088/0004-637X/776/2/67

Villanova, S., Carraro, G., & Saviane, I. 2009, A&A, 504, 845–852, doi: 10.1051/0004-6361/200811507

Wang, J., Chen, X., Deng, L., Zhang, J., & Sun, W. 2025, ApJ, 978, 53, doi: 10.3847/1538-4357/ad93b3

Wang, S., & Chen, X. 2019, ApJ, 877, 116, doi: 10.3847/1538-4357/ab1c61

Zhang, R., Wang, G.-J., Lu, Y., et al. 2024, A&A, 692, A212, doi: 10.1051/0004-6361/202450726

Zorec, J., & Royer, F. 2012, A&A, 537, A120, doi: 10.1051/0004-6361/201117691